Internal report to E89-003 collaboration

J.M. Udías and Javier R. Vignote
Departamento de Física Atómica, Molecular y Nuclear
Facultad de Ciencias Físicas, Universidad Complutense de Madrid, E-28040 Madrid, Spain
(February 8, 2001)

In all the following figures, the same kinematics is chosen: q-ω constant kinematics with, $|\vec{q}| \simeq 1$ GeV/c and $\omega = 445$ MeV. The beam energy is 2.445 GeV. The theoretical calculations have been fitted with the experimental cross section derived in [1]. The corresponding spectroscopy factors are quoted in Tables I to VI. We plot figures with cross section, asymmetry A_{TL} and R_{TL} response function for the two $1p$-shell of ^{16}O. For the $1p_{3/2}$ shell, a 100% contribution of the $(2s_{1/2}, 1d_{5/2})$ doublet has been also taken into account. An additional figure comparing different contributions of the doublet is plotted too. As the results tend to group together for the same operator ($cc1$ and $cc2$) [2], we plot in separate figures all the results with $cc1$ or $cc2$. If in the figures or in the tables it is not written another thing, the 'basis' options for the curves are:

1. kind of calculation: fully relativistic
2. bound nucleon wave function: NLSH [3].
3. optical potential: EDAI-O [4].
4. gauge: Coulomb
5. form factor model: Gari and Kun [5].
6. 100% contribution of the doublet included for the $p_{3/2}$ shell.

Starting from the above options, we modified some of them each time and compare the following ingredients:

1. **Relativistic** or not approach. This is shown in Figs. 1-4 for the two shells and two different kind of current operator option cc1 and cc2 [2]. We also show projected results that is, without the negative energy components what means most of the spinor distortion (but not all) is removed from the wave functions [6,7] and within EMA-noSV where all the spinor distortion is removed [8].
2. Different sets of **bound state wave function**. In Figs. 5-8 we compare fully relativistic results obtained with wave functions derived from different relativistic lagrangians: NLSH [3] and HS one [9] wave functions that differs principally in the predicted rms. We have also included results computed with a Lagrangian fine tuned so the wave functions reproduce the low-p data of Leuschner *et al.* [10] (NLSH-P).

3. **Gauge prescription.** We show in Figs. 9-12 results obtained within the fully relativistic formalism with different gauge prescriptions. The fully relativistic results are known to be more independent on the gauge prescription than the nonrelativistic, projected or EMA-noSV ones.

4. Different **optical potential**. In Figs. 13-16 we compare the results of different optical potentials available. For $T_F \simeq 400 MeV$ we have a rather large choice of optical potentials in the literature. We compute results with the following potentials: Purely phenomenological S-V potentials based upon Dirac equation, fitted to thousands of data points from elastic p-scattering from several nuclei [4]. The parameterization can be based on single nucleus (EDAI-O) data, or it can include an A-dependency fitted to several nuclei (EDAD1 and EDAD2). In Table V we also write the spectroscopic factor for two more optical potentials. MRW [11] and RLF [12].

5. **Form Factors**. A very small uncertainty is introduced through the nucleon form factors. Different models are compared in Figs. 17-20. Basically all the results are identical. Another issue is the possible density dependence of the nucleon form factors. We have computed results based on the form factors of Gari et al. [5] but with a density dependence similar to the one derived for the QMC form factors of ref. [13]. The change in the cross-section is rather modest. The effect of the density dependence of the form factor is visible in A_{TL} for $p_m > 300$ MeV.

6. **Contribution of the doublet**. In Fig. 21 we plot together three curves corresponding to different mixes of the doublet with the $1p_{3/2}$ shell. The spectroscopic factors are quoted in Table VII.

TABLES

Shell	Operator	Rel.		Proj.		EMA-noSV	
		S_α	χ^2/dof	S_α	χ^2/dof	S_α	χ^2/dof
$1p_{1/2}$	CC1	0.68(4)	5.5	0.78(8)	17.	0.72(3)	2.3
	CC2	0.74(3)	2.0	0.76(5)	8.0	0.75(3)	2.2
$1p_{3/2}$	CC1	0.62(3)	5.3	0.73(13)	79.	0.66(11)	65.
	CC2	0.67(8)	31.	0.71(12)	70.	0.69(11)	65.

TABLE I. Spectroscopic factors derived from J. Gao *et al.* experimental cross sections in reference [1] using three different types of calculation: full relativistic, projected over positive energies and EMA-noSV. Common variables are EDAI-O optical potential, NLSH bound nucleon wave function, Gari and Kun form factors and Coulomb gauge. The numbers within parentheses indicate the statistical error. The χ^2 per degree of freedom is also quoted.

Shell	Operator	NLSH		NLSH-P		HS	
		S_α	χ^2/dof	S_α	χ^2/dof	S_α	χ^2/dof
$1p_{1/2}$	CC1	0.68(4)	5.5	0.60(5)	10.	0.62(5)	10.
	CC2	0.74(3)	2.0	0.63(6)	15.	0.65(7)	18.
$1p_{3/2}$	CC1	0.62(3)	5.3	0.52(10)	97.	0.61(3)	6.7
	CC2	0.67(8)	31.	0.54(12)	115.	0.65(8)	41.

TABLE II. Spectroscopic factors derived from J. Gao *et al.* experimental cross sections in reference [1] using three different types of bound nucleon wave function: NLSH, NLSH-P and HS. Common variables are EDAI-O optical potential, full relativistic calculation, Gari and Kun form factors and Coulomb gauge. The numbers within parentheses indicate the statistical error. The χ^2 per degree of freedom is also quoted.

Shell	Operator	Coulomb		Weyl		Landau	
		S_α	χ^2/dof	S_α	χ^2/dof	S_α	χ^2/dof
$1p_{1/2}$	CC1	0.68(4)	5.5	0.63(8)	25.	0.69(3)	3.7
	CC2	0.74(3)	2.0	0.76(3)	2.6	0.73(3)	2.5
$1p_{3/2}$	CC1	0.62(3)	5.3	0.59(4)	9.2	0.63(3)	6.4
	CC2	0.67(8)	31.	0.70(7)	22.	0.67(8)	34.

TABLE III. Spectroscopic factors derived from J. Gao *et al.* experimental cross sections in reference [1] using three different choices of gauge: Coulomb, Weyl and Landau. Common variables are EDAI-O optical potential, full relativistic calculation, Gari and Kun form factors and NLSH bound nucleon wave function. The numbers within parentheses indicate the statistical error. The χ^2 per degree of freedom is also quoted.

Shell	Operator	EDAI-O		EDAD1		EDAD2	
		S_α	χ^2/dof	S_α	χ^2/dof	S_α	χ^2/dof
$1p_{1/2}$	CC1	0.68(4)	5.5	0.64(8)	29.	0.64(6)	15.
	CC2	0.74(3)	2.0	0.72(4)	4.8	0.71(1)	0.7
$1p_{3/2}$	CC1	0.62(3)	5.3	0.60(4)	12.	0.59(3)	6.4
	CC2	0.67(8)	31.	0.67(4)	8.2	0.65(5)	15.

TABLE IV. Spectroscopic factors derived from J. Gao *et al.* experimental cross sections in reference [1] using three different kinds of optical potential: EDAI-O, EDAD1 and EDAD2. Common variables are NLSH bound nucleon wave function, full relativistic calculation, Gari and Kun form factors and Coulomb gauge. The numbers within parentheses indicate the statistical error. The χ^2 per degree of freedom is also quoted.

Shell	Operator	EDAI-O		MRW		RLF	
		S_α	χ^2/dof	S_α	χ^2/dof	S_α	χ^2/dof
$1p_{1/2}$	CC1	0.68(4)	5.5	0.62(9)	35.	0.61(10)	41.
	CC2	0.74(3)	2.0	0.71(5)	7.6	0.70(4)	6.1
$1p_{3/2}$	CC1	0.62(3)	5.3	0.60(4)	11.	0.58(4)	12.
	CC2	0.67(8)	31.	0.67(4)	7.3	0.65(4)	7.9

TABLE V. Spectroscopic factors derived from J. Gao *et al.* experimental cross sections in reference [1] using three different kinds of optical potential: EDAI-O, MRW and RLF. Common variables are NLSH bound nucleon wave function, full relativistic calculation, Gari and Kun form factors and Coulomb gauge. The numbers within parentheses indicate the statistical error. The χ^2 per degree of freedom is also quoted.

Shell	Operator	GK		dipole		GK with QMC	
		S_α	χ^2/dof	S_α	χ^2/dof	S_α	χ^2/dof
$1p_{1/2}$	CC1	0.68(4)	5.5	0.69(4)	4.8	0.65(5)	11.
	CC2	0.74(3)	2.0	0.75(3)	2.1	0.72(1)	0.5
$1p_{3/2}$	CC1	0.62(3)	5.3	0.63(3)	5.9	0.61(2)	3.3
	CC2	0.67(8)	31.	0.68(8)	31.	0.66(5)	16.

TABLE VI. Spectroscopic factors derived from J. Gao *et al.* experimental cross sections in reference [1] using three different types of forms factors models: Gari and Kun, dipole and Gari and Kun with QMC. Common variables are EDAI-O optical potential, full relativistic calculation, NLSH bound nucleon wave function and Coulomb gauge. The numbers within parentheses indicate the statistical error. The χ^2 per degree of freedom is also quoted.

Shell	Operator	*sd* 100%		*sd* 50%		*sd* 0%	
		S_α	χ^2/dof	S_α	χ^2/dof	S_α	χ^2/dof
$1p_{3/2}$	CC1	0.62(3)	5.3	0.64(3)	6.1	0.66(3)	7.4
	CC2	0.67(8)	31.	0.70(8)	33.	0.72(8)	35.

TABLE VII. Spectroscopic factors derived from J. Gao *et al.* experimental cross sections in reference [1] using three different contributions of the doublet for the $1p_{3/2}$ shell: 100%, 50% and 0%. Common variables are EDAI-O optical potential, NLSH bound nucleon wave function, full relativistic calculation, Gari and Kun form factors and Coulomb gauge. The numbers within parentheses indicate the statistical error. The χ^2 per degree of freedom is also quoted.

REFERENCES

[1] J. Gao *et al.*, Phys. Rev. Lett. **84**, 3265 (2000).
[2] T. de Forest, Nucl. Phys. **A392** (1983) 232.
[3] M.M. Sharma, M.A. Nagarajan, P. Ring, Phys. Lett. B **312** (1993) 377.
[4] E.D. Cooper, S. Hama, B.C. Clark, R.L. Mercer, Phys. Rev. C **47** (1993) 297.
[5] Gari and Krumplemann, Z. Phys. A **322** (1985) 689.
[6] J.M. Udías *et al.*, Phys. Rev. Lett. **83** (1999) 5451.
[7] J.M. Udías, J.R. Vignote Phys. Rev C **62** (2000) 034302
[8] J.J. Kelly, Phys. Rev. C **56** (1997) 2672; *ibid.* **59** (1999) 3256.
[9] B.D. Serot and J.D. Walecka, Adv. Nucl. Phys. **16** (1986) 1.
[10] M. Leuschner *et al.*, Phys. Rev. C **49** (1994) 955.
[11] J.A. McNeil, L. Ray and S.J. Wallace, Phys. Rev. C **27** (1983) 2123.
[12] C.J. Horowitz, Phys. Rev. C **31** (1985) 1340; D.P. Murdock and C.J. Horowitz, Phys. Rev. C **35** (1987) 1442.
[13] Lu *et al.*, Phys. Lett. B **417** (1998) 217; Phys. Rev. C **60** (1999) 068201.

FIGURES

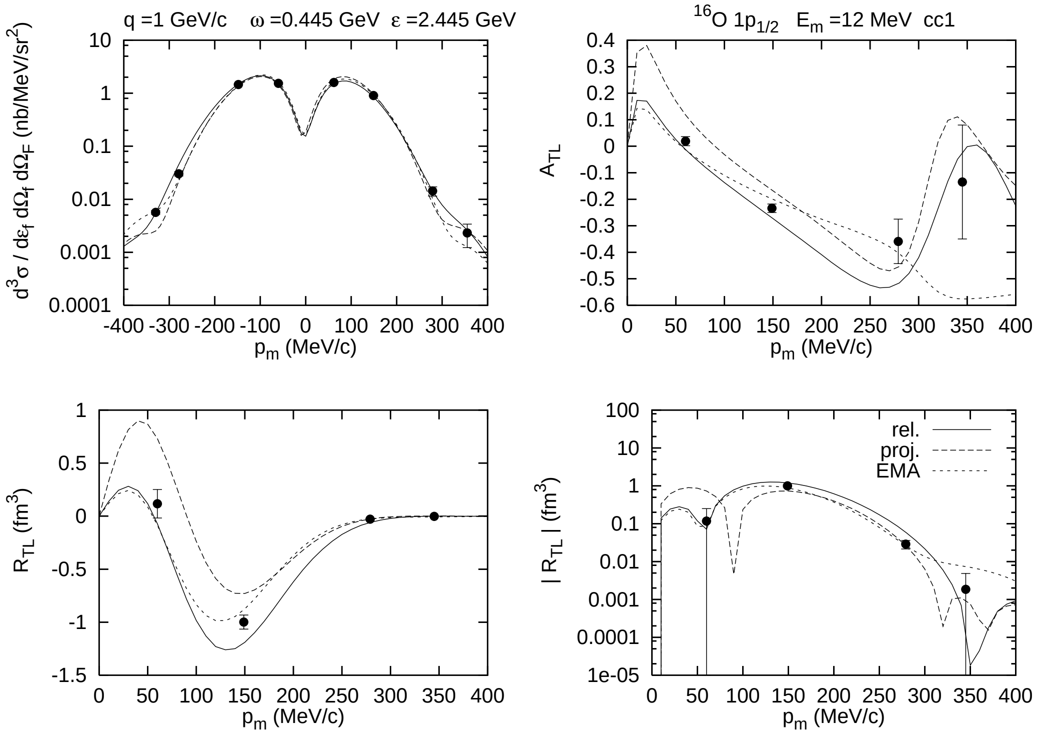

FIG. 1. Calculations for cross section, A_{TL} asymmetry and R_{TL} response function compared to experimental results from [1]. Shell $1p_{1/2}$, kind of current operator $cc1$. Solid line full relativistic calculation, long-dashed projection over positive energies and short-dashed EMA-noSV.

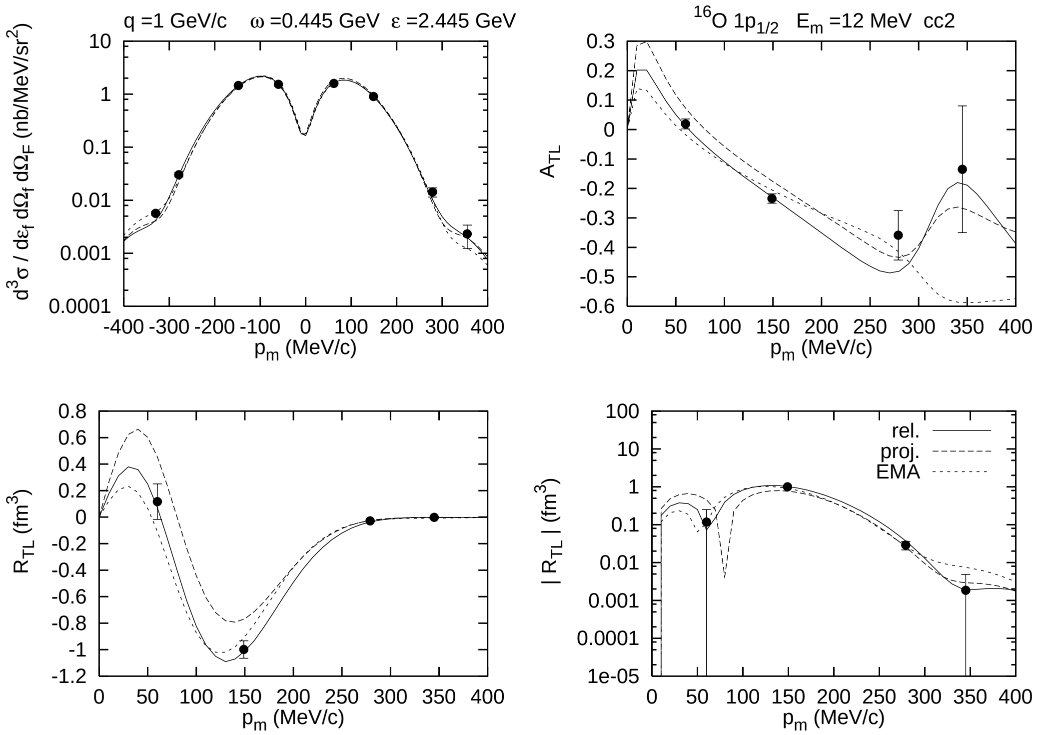

FIG. 2. Same as Fig. 1 but current operator $cc2$.

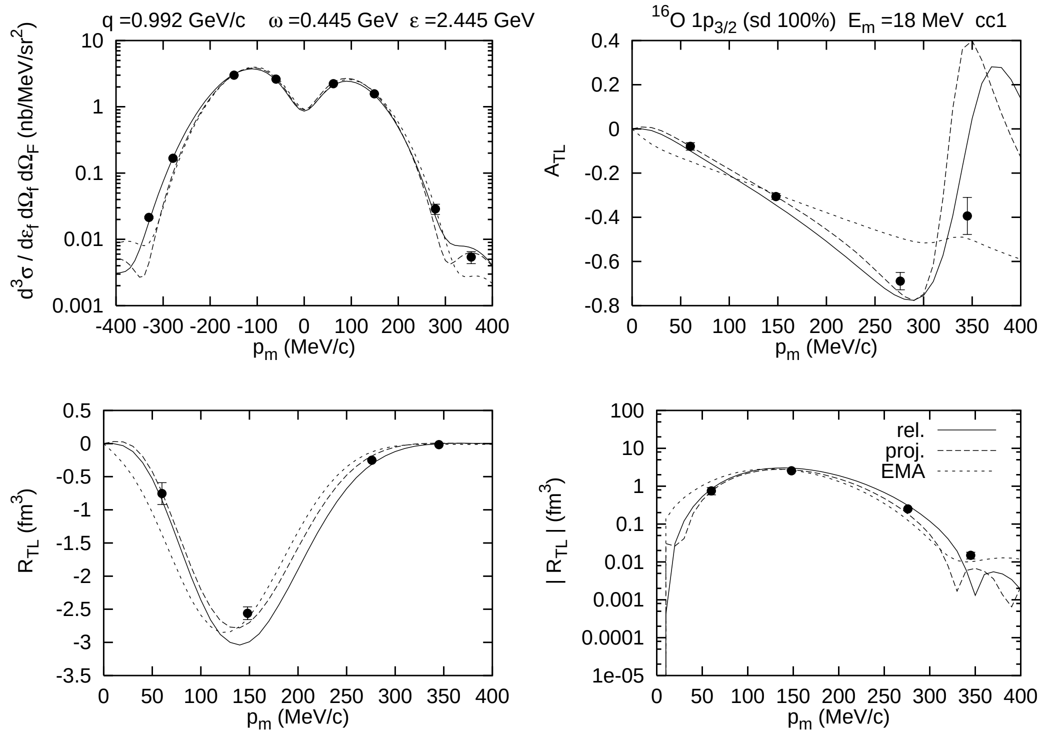

FIG. 3. As Fig. 1 now for $p_{3/2}$ shell.

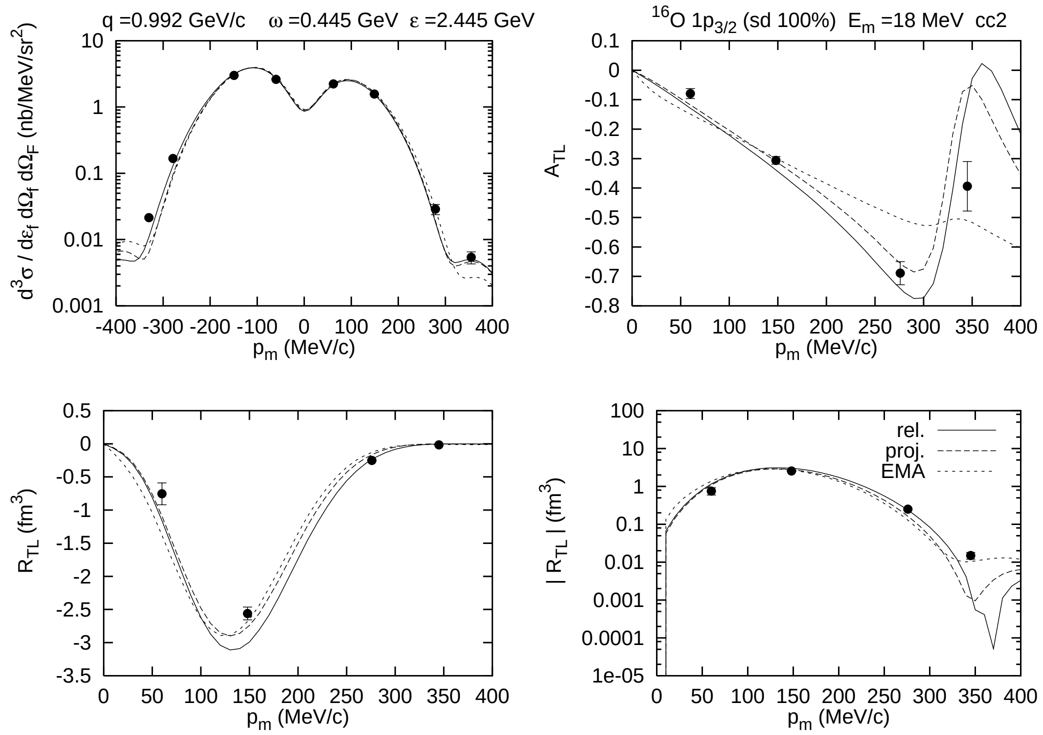

FIG. 4. As Fig. 2 now for $p_{3/2}$ shell.

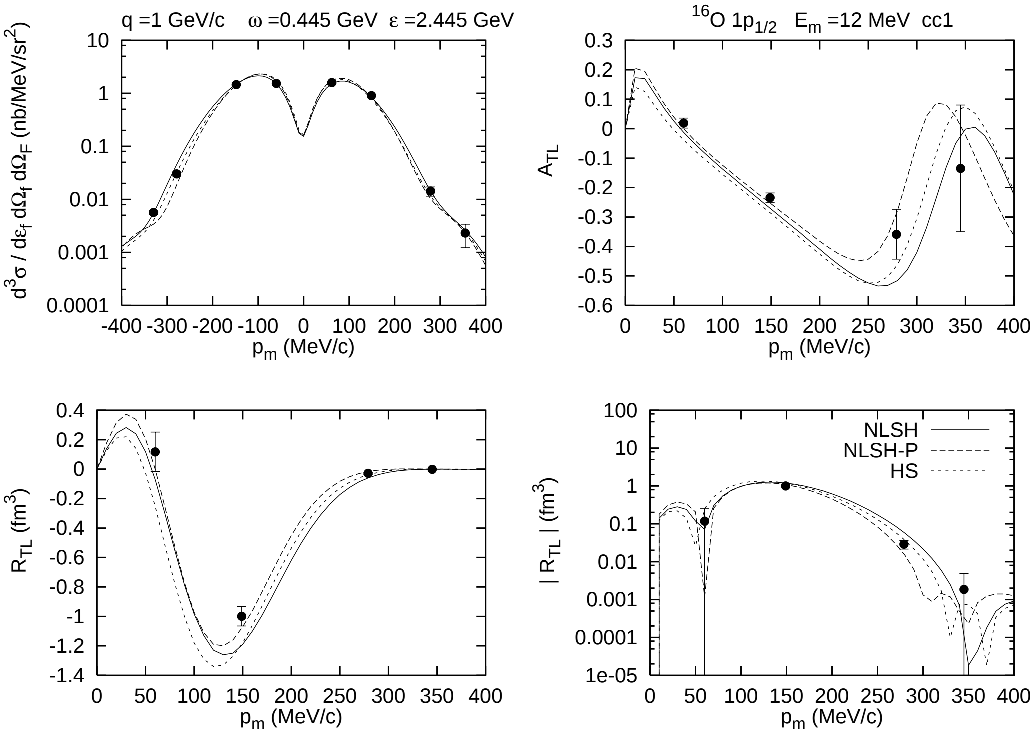

FIG. 5. Now comparing different kind of bound nucleon wave functions. Solid NLSH, long-dashed NLSH-P and short-dashed HS.

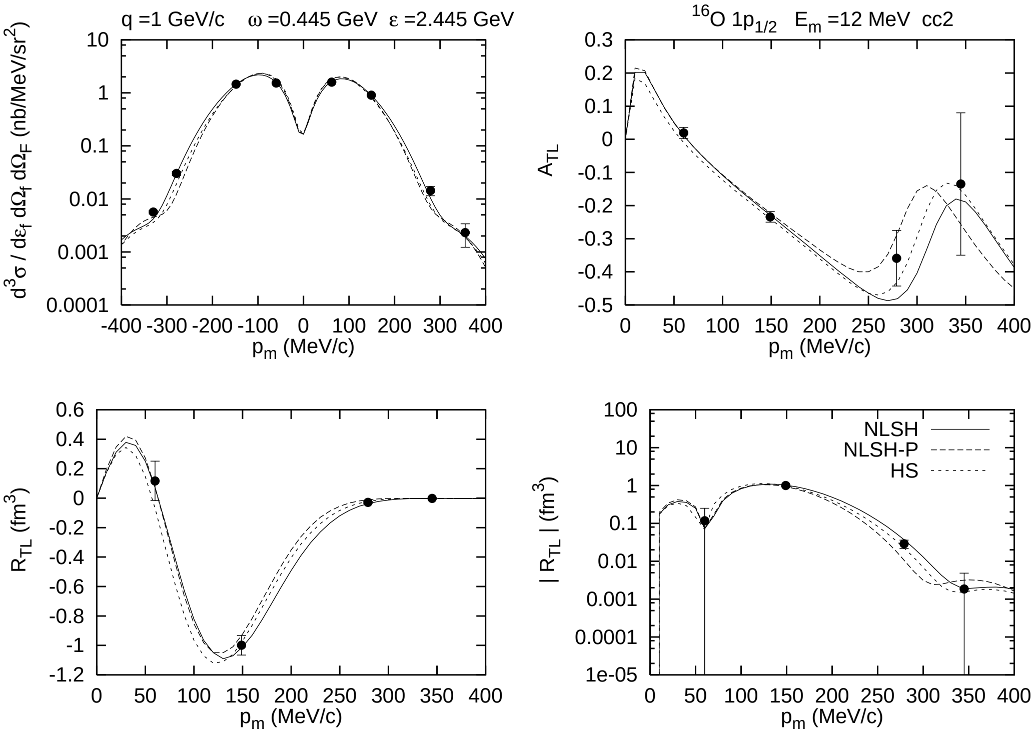

FIG. 6. As Figure 5 above for $cc2$.

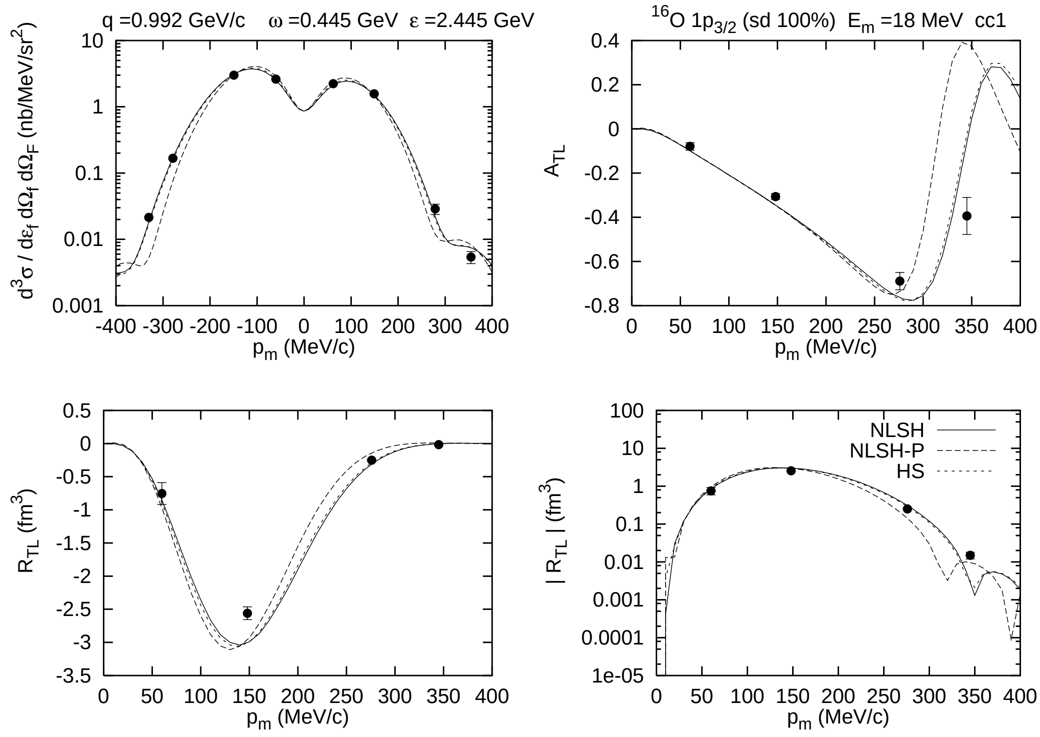

FIG. 7. Same as Figure 5 for $p_{3/2}$ shell.

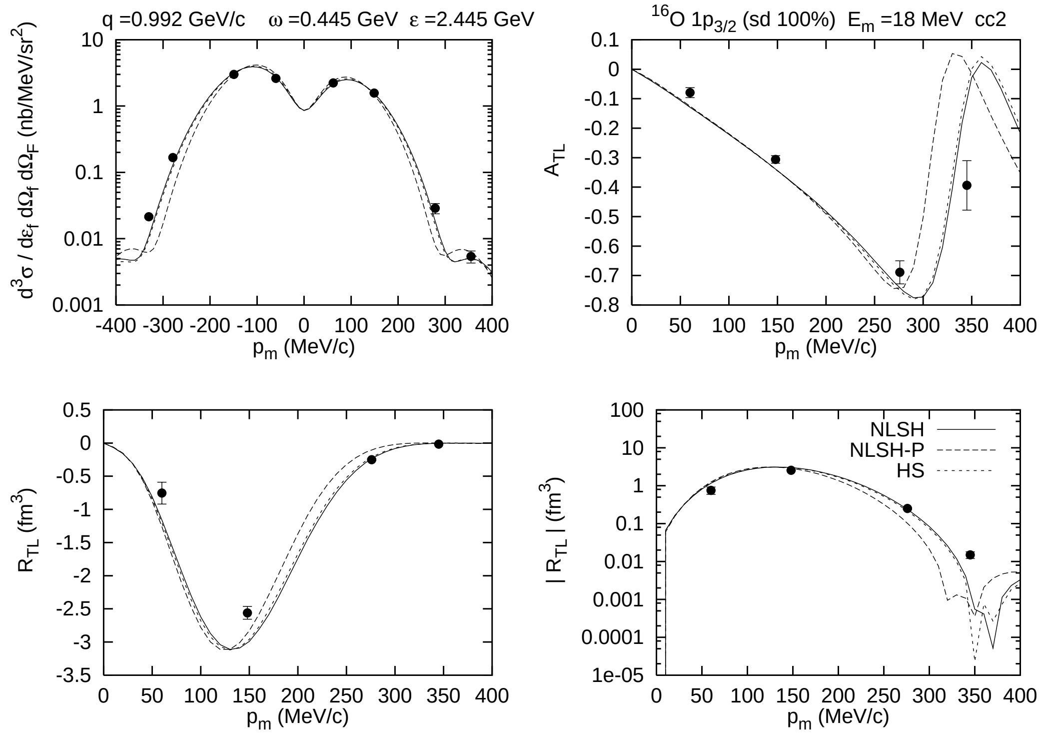

FIG. 8. As Fig. 7 for $cc2$.

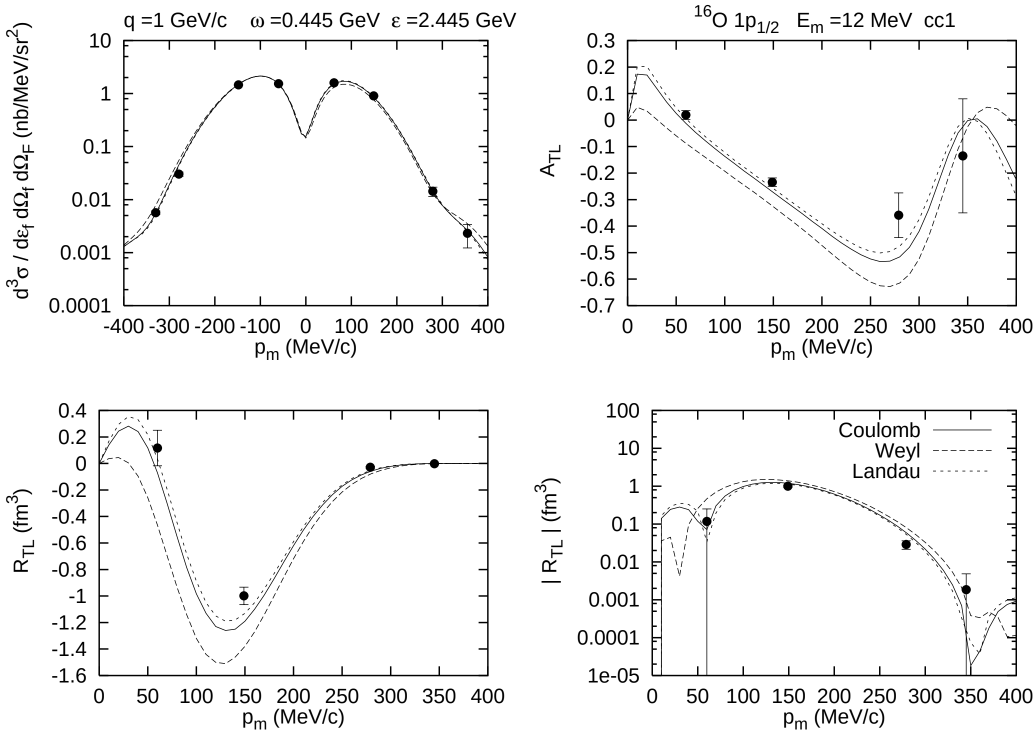

FIG. 9. Three kinds of gauges. Solid Coulomb gauge, long-dashed Weyl gauge and short-dashed Landau gauge.

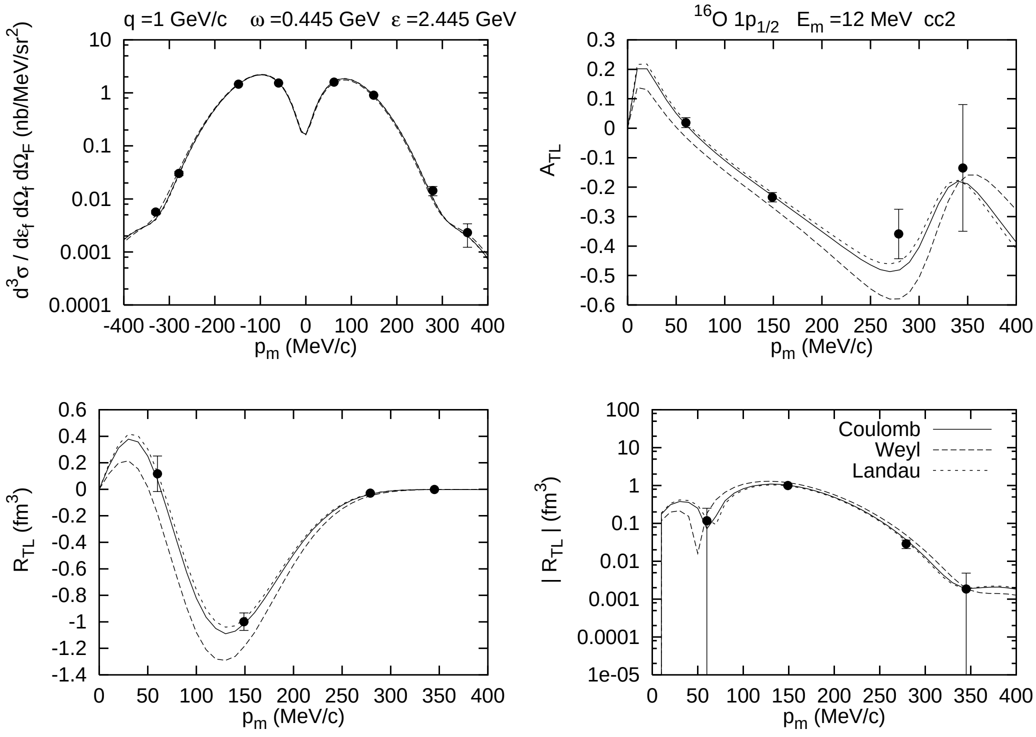

FIG. 10. As Fig 9 for $cc2$.

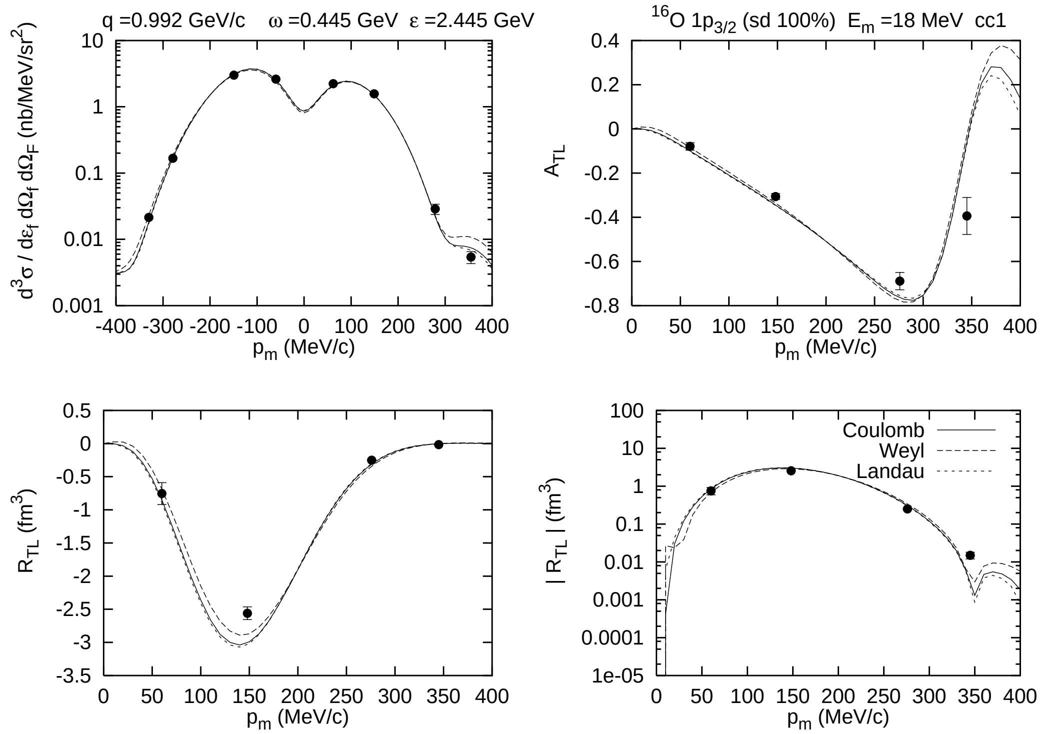

FIG. 11. Same as Figure 9 for $p_{3/2}$ shell.

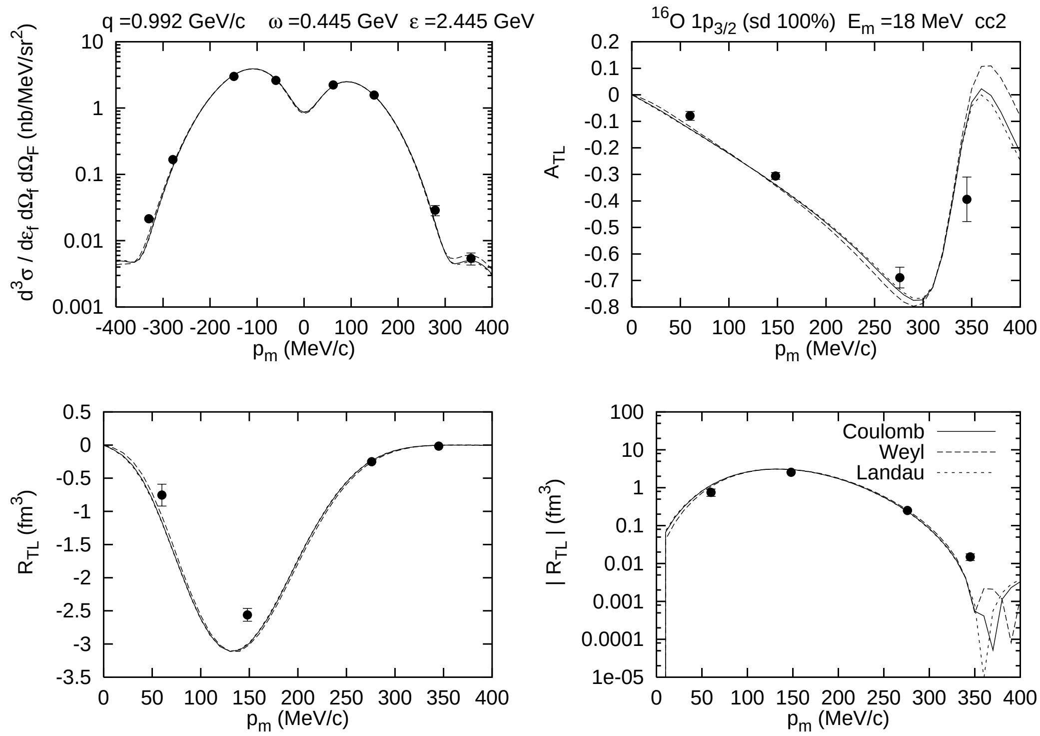

FIG. 12. As Fig. 11 for $cc2$.

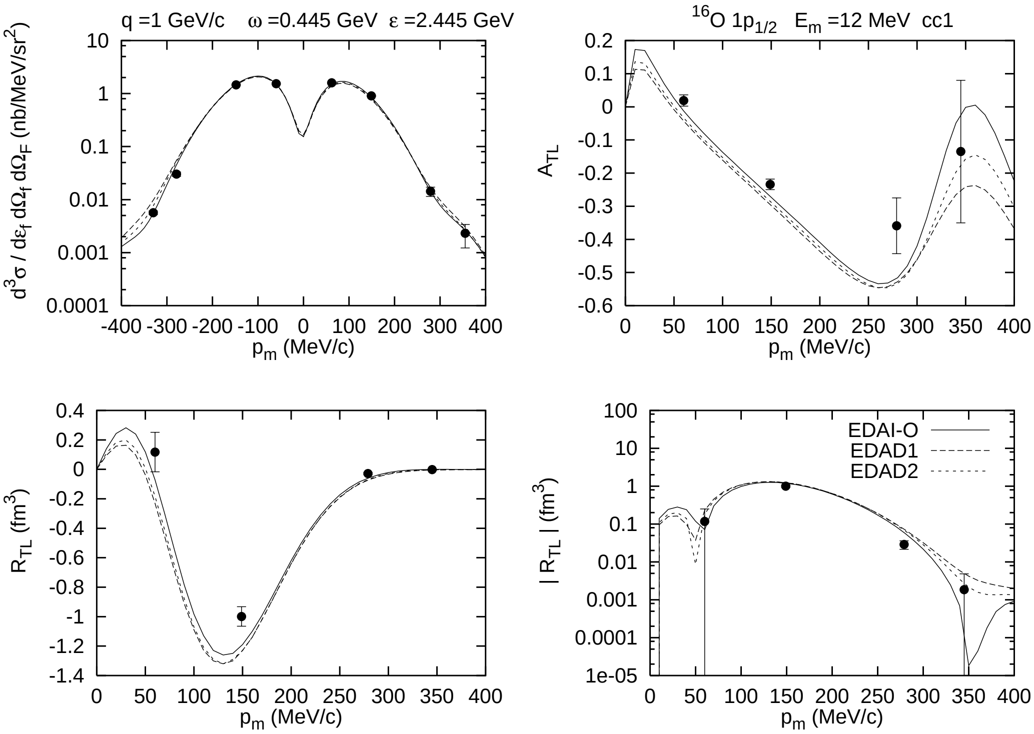

FIG. 13. Three kinds of optical potentials now. Solid EDAI-O, long-dashed EDAD1 and short-dashed EDAD2.

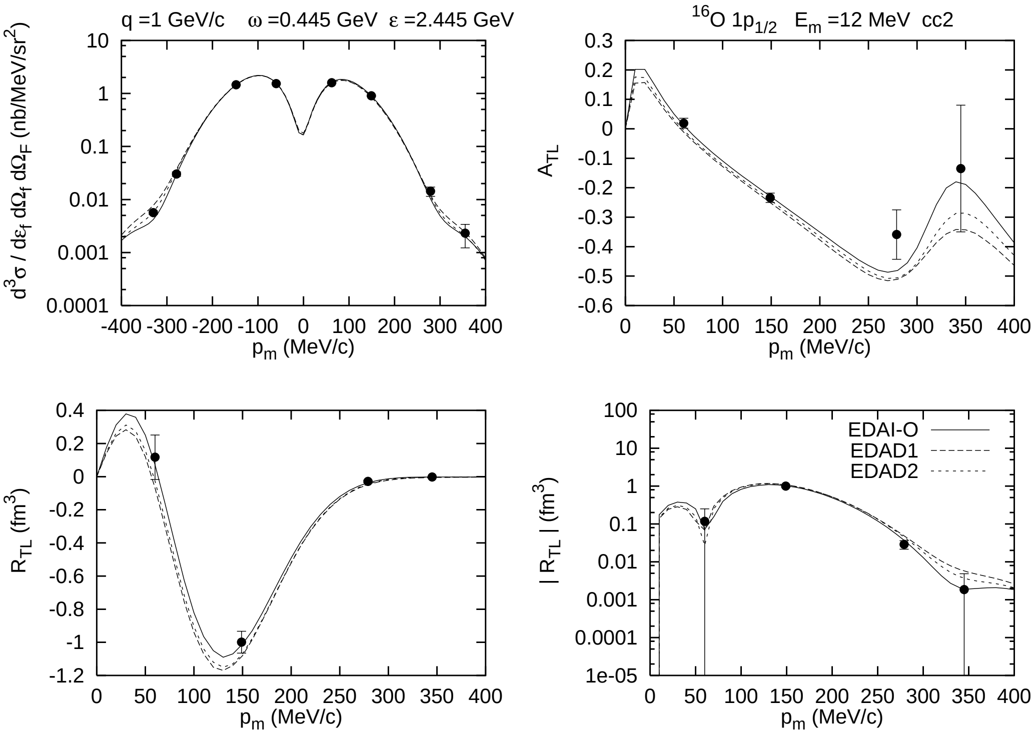

FIG. 14. As Fig 13 for *cc*2.

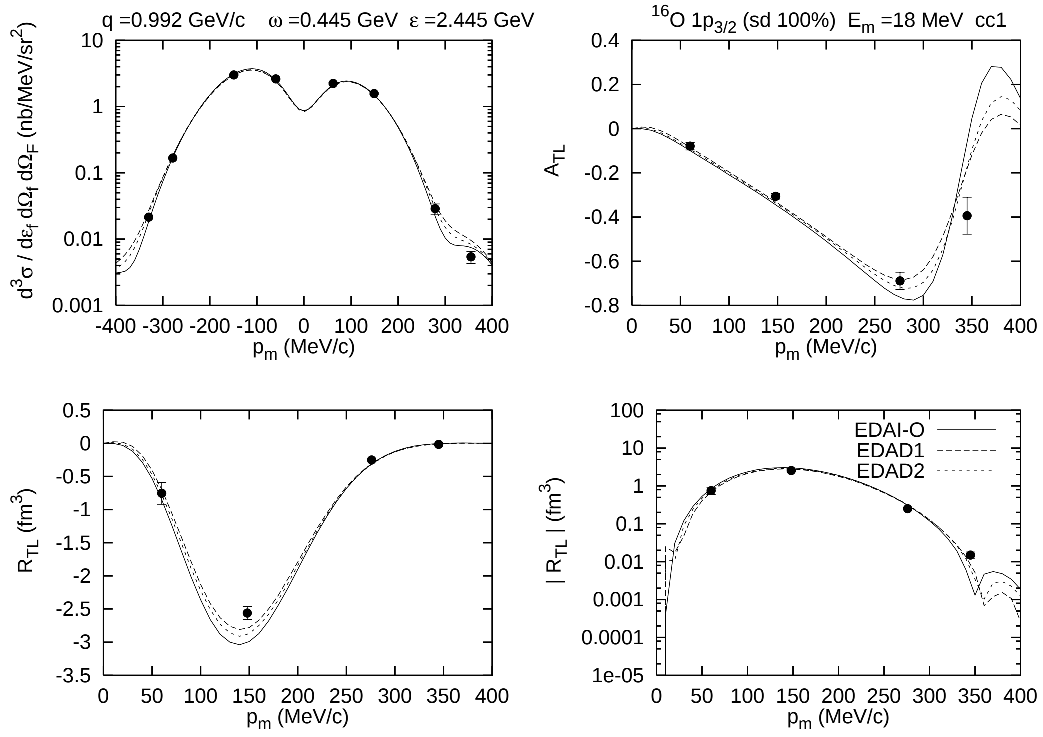

FIG. 15. Same as Figure 13 for $p_{3/2}$ shell.

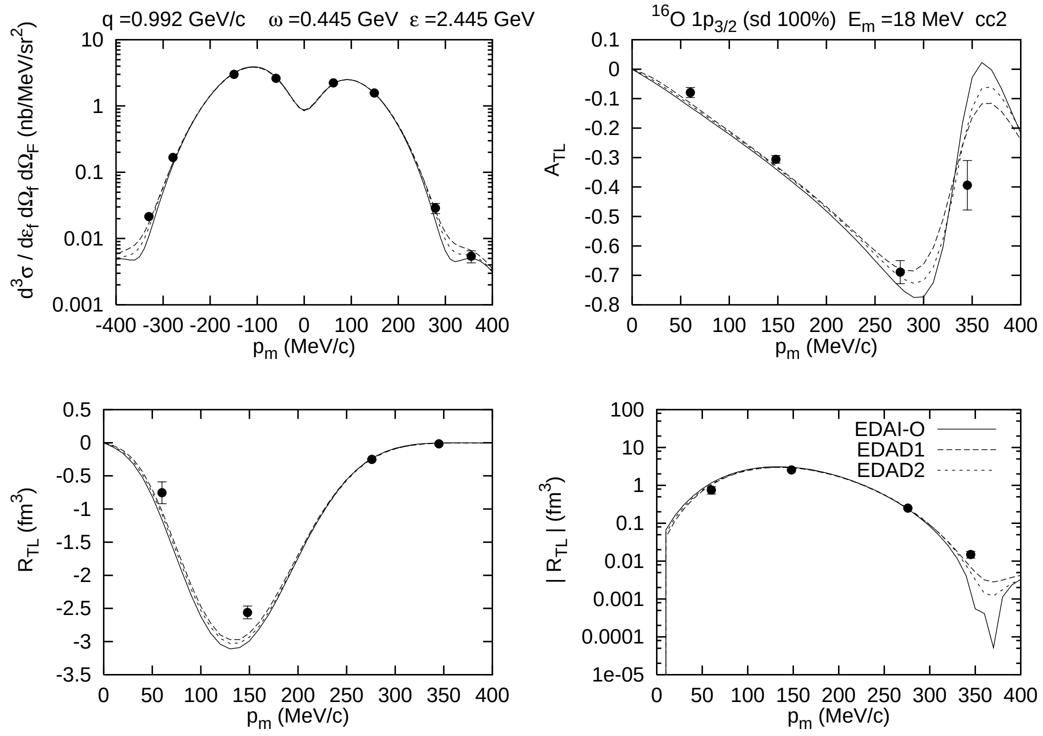

FIG. 16. As Fig. 15 for $cc2$.

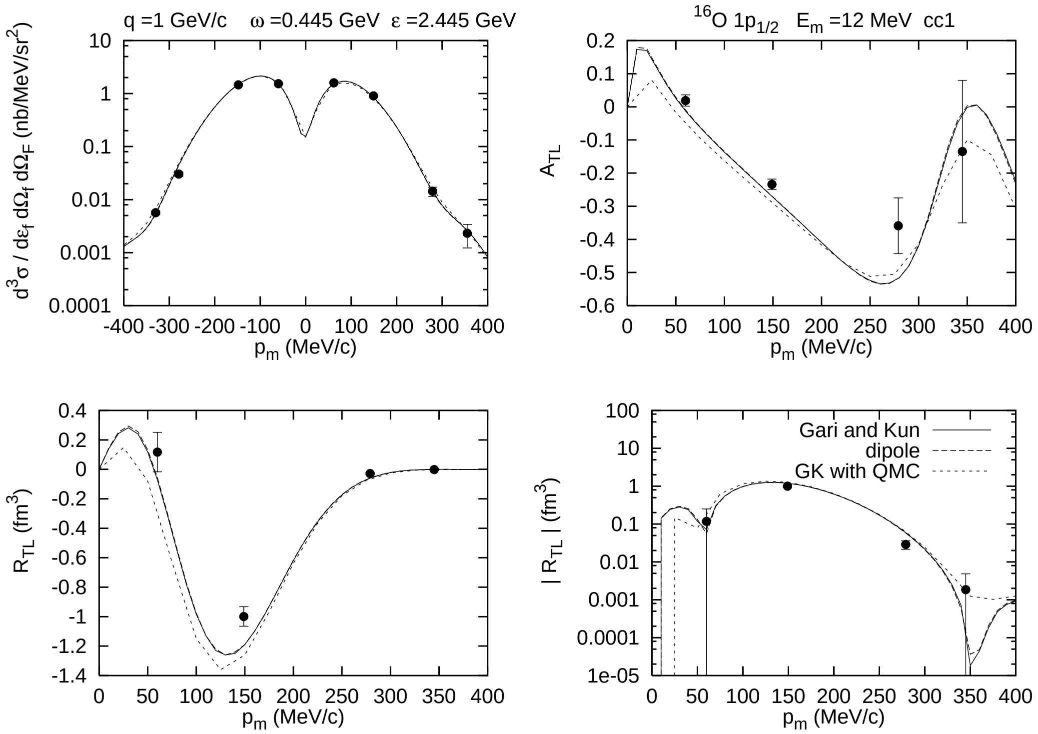

FIG. 17. Different form factors, solid line Gari and Kun form factors, long-dashed line dipole form factors and short-dashed Gari a Kun with QMC.

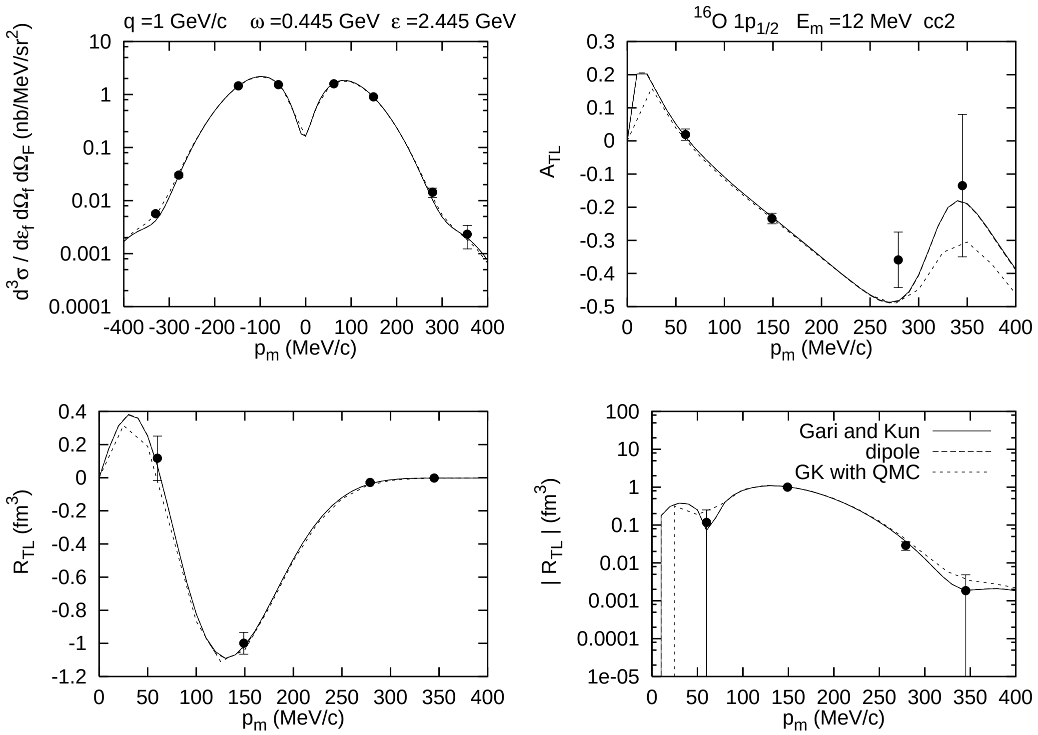

FIG. 18. As Fig 17 for $cc2$.

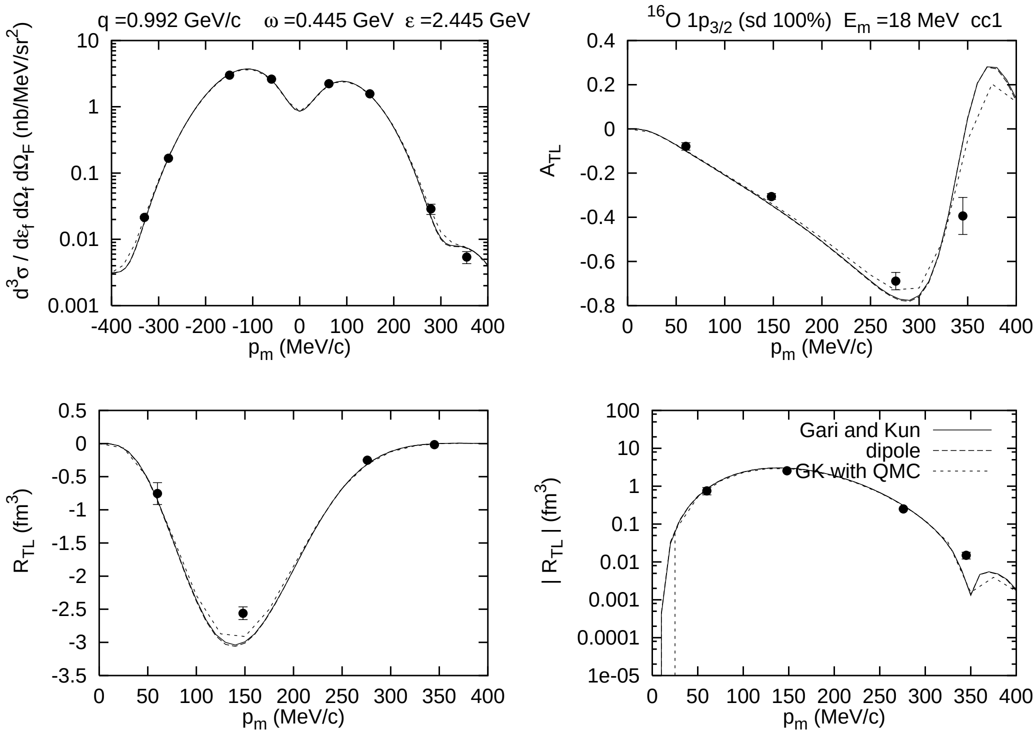

FIG. 19. Same as Fig. 17 for $p_{3/2}$ shell.

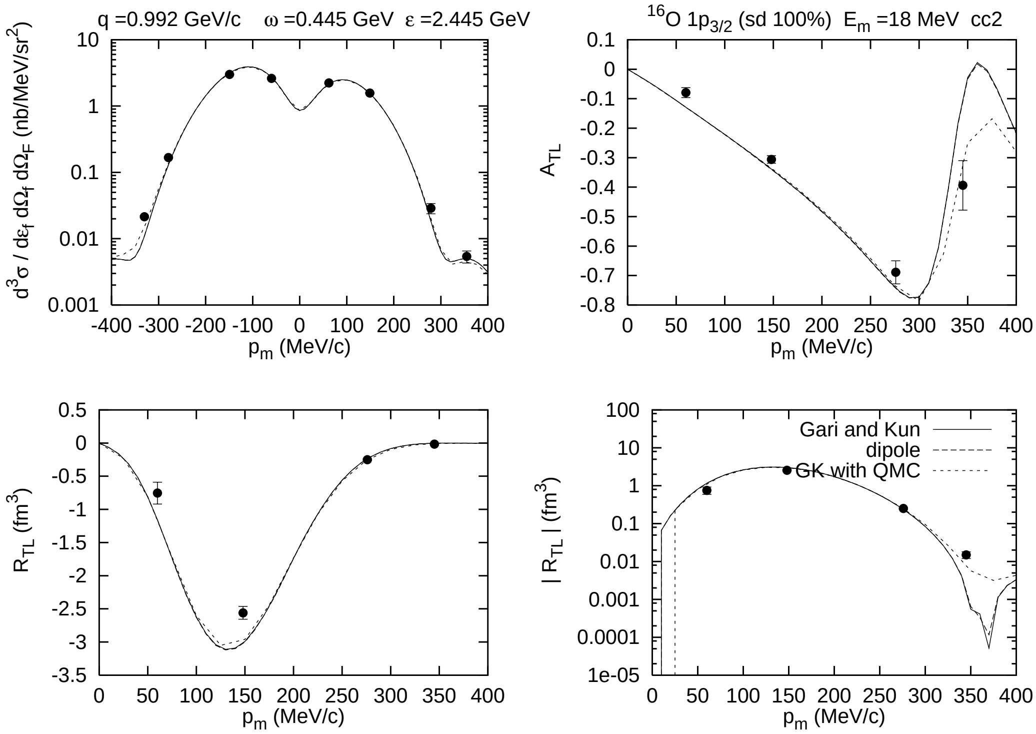

FIG. 20. As Fig. 19 for *cc*2.

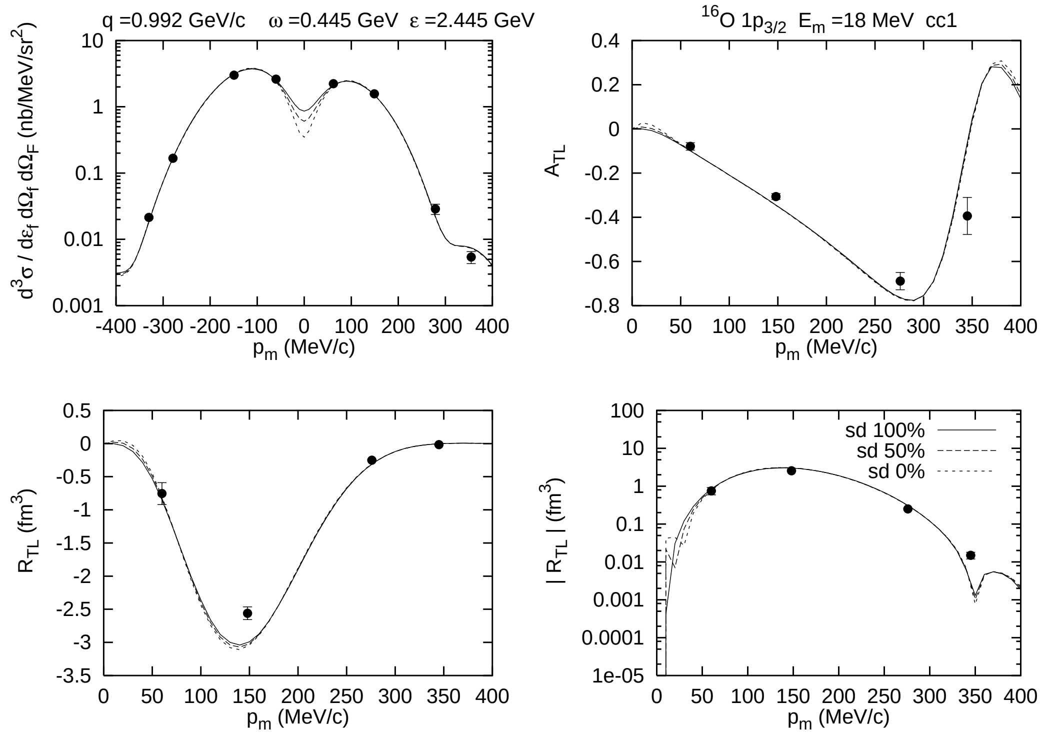

FIG. 21. Different contributions of the $(2s_{1/2}, 1d_{5/2})$ doublet for the $1p_{3/2}$ shell. Solid 100%, long-dashed 50% and short-dashed 0%.

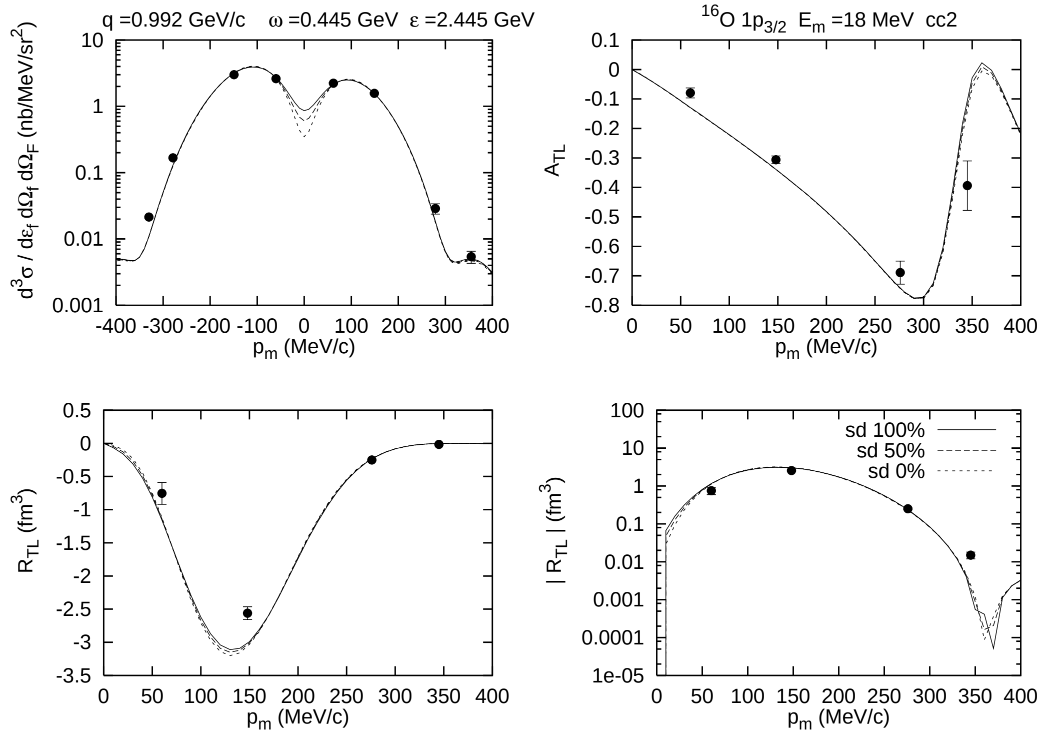

FIG. 22. As Fig. 21 for $cc2$.